



CHORUS

This is the accepted manuscript made available via CHORUS. The article has been published as:

High harmonic generation in magnetically-doped topological insulators

Lei Jia, Zhiya Zhang, D. Z. Yang, M. S. Si, G. P. Zhang, and Y. S. Liu

Phys. Rev. B **100**, 125144 — Published 20 September 2019

DOI: [10.1103/PhysRevB.100.125144](https://doi.org/10.1103/PhysRevB.100.125144)

High harmonic generation in magnetically doped topological insulators

Lei Jia, Zhiya Zhang, D. Z. Yang, and M. S. Si*

*Key Laboratory for Magnetism and Magnetic Materials of the Ministry of Education,
Lanzhou University, Lanzhou 730000,
China & Key Laboratory of Special Function Materials
and Structure Design of Ministry of Education,
Lanzhou University, Lanzhou 730000, China*

G. P. Zhang[†]

Department of Physics, Indiana State University, Terre Haute, IN 47809, USA

Y. S. Liu

*College of Physics and Electronic Engineering,
Changshu Institute of Technology, Changshu 215500, China*

(Dated: September 6, 2019)

Abstract

As a new class of condensed matter, topological insulators challenge the traditional wisdom of condensed matter physics. Doping topological insulators with magnetic elements can realize the quantum anomalous Hall state, a two-dimensional bulk insulator with non-zero Chern number. High harmonic generation (HHG) has emerged as a very promising tool to probe electronic properties. However, its application to magnetically doped topological insulators has not been realized. Here, we predict that high harmonics from six quintuple layers of Bi_2Se_3 (6QL- Bi_2Se_3) carry crucial information about its structure. HHG sensitively depends on crystal symmetry and laser polarization. While in the parent compound 6QL- Bi_2Se_3 all the harmonic orders are odd, once it is doped with a magnetic Cr atom, selective even and odd harmonics appear, depending on whether the laser field is in-plane or out-of-plane. With spin-orbit coupling, both even and odd harmonics appear. We find that these seemingly complicated harmonics have a simple origin: microscopic interplay between symmetry operations and laser polarization. Our finding demonstrates the unexplored power of HHG in topological insulators and will have a broad impact on future research.

I. INTRODUCTION

Probing electronic properties and symmetry properties of solids by means of high harmonic generation (HHG) is new and has attracted worldwide attentions [1–5]. In contrast to gas-phase HHG [6], high-order harmonics can be generated under a relatively weak laser field in solids [7], benefiting from high density in solids. This is the cornerstone of attosecond science [8]. However, the electronic properties in solids are more complex, so is HHG. Earlier solid-state HHGs were mainly found in semiconductors or/and insulators [9]. The mechanism is attributed to Bloch oscillations that involve intra- and inter-band electron dynamics [10]. Han *et al.* have successfully extended HHG into metals [11]. The underlying physics is well described by the Sommerfeld model of a free-electron gas. By contrast to the classification of insulators, semiconductors and metals in terms of the band theory, a new quantum phase called topological insulator (TI) arises due to the protection of topological invariant, challenging the traditional understanding of condensed matter physics [12]. Interestingly, Hsieh *et al.* experimentally observed the surface second harmonic generation from TI Bi_2Se_3 , which stems from the broken inversion symmetry induced by the perpendicular surface electric field [13]. In addition, Avetissian *et al.* pointed out HHG can be realized in three-dimensional TI [14], where the confined two-dimensional metallic carriers emit the coherent electromagnetic radiation. Most recently, Zhang *et al.* reported that magnetic materials have a spin-polarized HHG [15]. It is well known that magnetically doped TIs would lead to a gaped edge or surface state [16], offering an ideal platform to study the quantum anomalous Hall effect [17–19]. However, little is known about HHG in magnetically doped TIs.

In this work, we predict that a topological insulator, once doped with a magnetic atom, has very peculiar high harmonic signals. We take 6 quintuple layers of Bi_2Se_3 (6QL- Bi_2Se_3) as an example, and find that under a moderate laser field, the highest harmonic order reaches 13. These harmonics show a strong laser-polarization dependence, reflecting the exotic topological influence. Once 6QL- Bi_2Se_3 is doped with a magnetic Cr atom, the newly induced spin polarization and symmetry reduction bring in even harmonics only when the laser polarization is along either the x or z axis. When the laser polarization is along the y axis, harmonic orders are even along the x axis. To fully understand the physics behind these peculiar harmonic signal changes, we examine the group symmetry before and after

doping. Before doping 6QL-Bi₂Se₃ has 12 symmetry operations, which are inequivalent once a specific laser polarization is chosen. We discover that these 12 symmetry operations form three subgroups, with four members in each subgroup. The laser polarization further split the subgroups into units. The harmonic signals are a result of a joint effect of symmetry operations within each unit. Once doped with a Cr atom, the system loses 6 symmetry operations and also the inversion symmetry, and the laser polarization groups a new set of constituents in each unit. Our finding is a rare manifestation of the interplay between topological structural information and laser polarization in high-order harmonic generation. This paves the way to future applications of HHG as an accurate tool to probe electronic and magnetic properties in exotic materials.

II. ALGORITHM

Bi₂Se₃ is a three-dimensional TI, and exhibits exotic electronic properties. Bi₂Se₃ crystallizes in a rhombohedral structure with the space group D_{3d}^5 , as shown in Fig. 1(a). We can see that Bi₂Se₃ is layer-stacked from the repeated QL, which is mediated by van der Waals interaction. The crystal has the three-fold rotational symmetry with the trigonal axis defined as the z axis, the reflection symmetry with a bisect axis as the x axis, and the two-fold rotational symmetry with the binary axis as the y axis. We perform first-principles calculations using the Wien2k code [20], which adheres to the strict crystal symmetry. We use parameters similar to Ref. [21], and solve the Kohn-Sham equation to get the eigenstates and eigenenergies. Figure 1(b) demonstrates that the band structure has a gaped bulk phase. Due to the strong spin-orbit coupling (SOC), the band inversion occurs at the Γ point, producing a energy gap of around 0.4 eV [22]. Experimentally Bi₂Se₃ can be easily cleaved along the z axis and topological surface states appear. We use 6QL-Bi₂Se₃ to reproduce the topological states. The calculated surface electronic structure in Fig. 1(c) shows that the robust surface metallic bands cross the Fermi level.

Once we obtain the Bloch wavefunction $\psi_{i\mathbf{k}}(r)$ for band i and crystal momentum \mathbf{k} , we construct the density matrix of the ground state through $\rho_0 = \psi_{i\mathbf{k}}^*(r)\psi_{i\mathbf{k}}(r)$ for the dynamic calculations. We emphasize that all the calculations of electronic properties and HHGs use three dimensional real materials Bi₂Se₃, 6QL-Bi₂Se₃, and Cr-doped 6QL-Bi₂Se₃. We do not use a one-dimensional model. Under irradiation of light, the dynamic density matrix ρ is

computed from the time-dependent Liouville equation, which reads

$$i\hbar\langle i\mathbf{k}|\frac{\partial\rho}{\partial t}|j\mathbf{k}\rangle = \langle i\mathbf{k}|H_0 + H_I, \rho|j\mathbf{k}\rangle, \quad (1)$$

where H_0 is the system Hamiltonian and H_I is the interaction between the system and laser field: $H_I = \gamma\hat{\mathbf{P}} \cdot \mathbf{A}(t)$, where γ is the charge-mass ratio of electron, $\hat{\mathbf{P}}$ is the momentum operator, and $\mathbf{A}(t)$ is the vector potential of light field. The time-dependent macroscopic polarization $\mathbf{P}(t)$ is computed from $\mathbf{P}(t) = \sum_k \text{Tr}[\rho_k(t)\hat{\mathbf{P}}_k]$, where the trace is over band indices. Finally, HHG is computed by Fourier transforming $\mathbf{P}(t)$ into the frequency domain through,

$$\mathbf{P}(\Omega) = \int_{-\infty}^{\infty} \mathbf{P}(t)e^{i\Omega t} dt, \quad (2)$$

where Ω is the harmonic frequency. The duration of our femtosecond laser pulse is set to 60 fs, and two photon energies of 1.0 and 1.5 eV are used. [The vector potential of the electric field is taken as \$A_0 = 0.03 \text{ Vfs}/\text{\AA}\$](#) . This unit can be converted to the standard unit of $\text{V}/\text{\AA}$ by multiplying A_0 by the photon frequency ω (fs^{-1}). The converted electric fields are respectively 0.046 and 0.069 $\text{V}/\text{\AA}$, comparable to the experimental values. Other parameters give very similar results, as demonstrated in Supplemental Material [23].

III. RESULTS AND DISCUSSIONS

A. Harmonic signals

We show high-order harmonics generated from 6QL-Bi₂Se₃ with the laser polarization along the x , y , and z axes in Figs. 1(d)-1(f), respectively. Signals at noise level are not shown. The harmonic order reaches at least 13. Figure 1(d) shows that if the laser electric field is along the x axis, the emitted harmonic signal is only polarized along the x or z axis. However, if the laser electric field is along either the y or z axis, the emitted harmonics are polarized along the y and z , respectively, (see Figs. 1(e) and 1(f)). All the harmonics are odd. The laser polarization along the x and y does not give the same result. This reminds us of the importance of the group symmetry in HHG [4]. To fully understand these results, we analyze the symmetry group of 6QL-Bi₂Se₃.

While in the traditional nonlinear optics the symmetry properties for low harmonics are known [24], there are very few discussions in the literature [25–28], most of which do not

pertain to actual crystals that usually have complicated symmetry groups [29]. However, we find a way to pin down the origin of these peculiar harmonics. We follow the laser polarization and classify the 12 symmetry operations in 6QL-Bi₂Se₃ into three subgroups (SGs), as shown in Tab. I. Within each subgroup, two symmetry operations form a unit, but which two form the unit is determined by the polarization of laser field with respect to the crystal axis. The two symmetry operations in the unit can either leave the laser field intact or just reverse it. We take SG_I as an example. When the laser field is polarized along the x axis, E and σ_{xz} form a unit while I and R_y form another. Within the same unit, each symmetry operation has the same effect on the laser polarization. For the unit of E and σ_{xz} , they leave the x -polarized laser field unchanged, while another unit of I and R_y reverses the direction of the laser polarization. This has an important consequence on the selection of harmonic signals. E and σ_{xz} jointly cancel out the y -component of harmonics, while keep the x - and z -component of harmonics. The case is also true for the unit of I and R_y . We should point out that each of four symmetry operations, E , σ_{xz} , I , and R_y , can generate both even- and odd-order harmonics alone. Once the other operation in the same unit appears, the even-order harmonics is eliminated because the inversion symmetry is then correctly restored when these four symmetry operations are included. This requires us to rigorously include the symmetry properties.

When the laser field is along the y axis, E partners with R_y to form a unit, while I and σ_{xz} form another one. Each unit cancels out harmonics along the x and z axes, and keeps that along the y axis. The same principle also holds for the laser field polarized along the z axis. Two units of symmetry operations are the same as those when the laser field is polarized along the x axis.

B. Impact from Cr-doped 6QL-Bi₂Se₃

All the harmonics from the pristine TI 6QL-Bi₂Se₃ are normal. However, it is no longer the case for Cr doping. Following the work by Fang and coworkers [19], we employ Cr-doped 6QL-Bi₂Se₃ (inset of Fig. 2(a)) as our model system. Once the Cr atom is introduced, the density of states (DOS) near the Fermi level is exchange-split. The corresponding HHG is spin-dependent [15], protected by the time reversal breaking. The spin-polarized HHGs for the spin up channel are displayed in Figs. 2(a)-2(c). Since the inversion symmetry is broken

due to the magnetic doping, the original 12 symmetry operations are reduced to 6, and each subgroup only has two symmetry operations. For SG_I , only E and σ_{xz} remain, losing I and R_y . The other four symmetry operations form two groups: SG_{II} includes symmetry operations C_3^1 and σ_1 , while SG_{III} includes C_3^2 and σ_2 . The reduced symmetries have a dramatic impact on HHG.

We first align the laser polarization along the x axis. According to the above symmetry analysis, E and σ_{xz} form a unit. This combination cancels out any harmonic signals along the y axis, while the x - and z -components remain. Figure 2(a) shows that both the even- and odd-order harmonics appear because the inversion symmetry is broken.

However, when we align the laser polarization along the y axis, we observe the harmonic signals qualitatively different from the above x polarization result. The harmonics generated along the y axis (i.e., the laser polarization direction) only have odd orders. But the signals along the x and z axes are all even. In other words, the harmonic orders with signals along the original laser polarization are odd, but the harmonic orders with signals perpendicular to the original laser polarization are even.

When the laser field is polarized along the z axis, harmonics appear only along the z axis, and the other two components are canceled out (see Fig. 2(c)). In this case, the in-plane orthorhombic symmetries D_3 are preserved regardless of the linearly z -polarized laser field. Meanwhile, we can also see this from 6 remaining symmetry operations, which cannot change the z -polarized laser field. As a consequence, the in-plane signals are canceled out from the joint effect of the 6 symmetry operations. By contrast, due to the lack of inversion symmetry, the out-of-plane signals include both the even- and odd-order harmonics. For the spin down channel, the spin-polarized HHGs are similar to those of spin up channel. The only difference is the relative smaller intensity, which originates from the spin-polarized DOS near the Fermi level [15].

Symmetry effects on harmonics have been reported in gallium selenide [30], and also in monolayer transition metal dichalcogenides [31]. However, these studies failed to give any plausible explanations. Here we try to demonstrate the underlying mechanisms based on crystal symmetry. We use the laser polarization along the y axis as an example, with the same laser parameters as those in Fig. 2(b). We find the key reason for the unusual harmonics is that E and σ_{xz} no longer form a unit. This is because the laser polarization breaks the in-plane crystal symmetry, that is the reflection symmetry along the x axis (see

the right bottom panel of Fig. 1(a)). We can reveal further insights into these peculiar harmonics by resolving harmonic signals along different crystal momentum directions. We take the Γ point and examine the contribution of each symmetry operation to the harmonic signal separately. We note in passing that for each symmetry operator O , the interaction Hamiltonian is $H_I^O = \gamma O \hat{\mathbf{P}} \cdot \mathbf{A}(t)$ [15], so the calculated polarization $\mathbf{P}^O(t)$ depends on O , and the power spectrum becomes symmetry-resolved.

Figure 2(d) shows the symmetry-resolved harmonic signals emitted along the x axis. We see that E and σ_{xz} separately yield both even- and odd-order harmonics. Interestingly, the even-order signals are much stronger than the odd-order ones. When both E and σ_{xz} are present, the smaller odd-order harmonics cancel out. If we apply this rule to SG_{II} , we find the same results (see the blue line in Fig. 2(d)). When we include all the 6 symmetry operations, only the even-order signals appear, similar to the total one (see Fig. 2(b)). Figure 2(e) shows the symmetry-resolved y -component of harmonic signals. Then we include E or σ_{xz} separately, both the even- and odd-order signals occur. However, in this case, the even-order signals are much weaker than the odd-order ones. When both E and σ_{xz} are included, the weaker even-order signals disappear. Different types of harmonics along the x and y axes can be understood from the cooperation of E and σ_{xz} , protected by the reflection symmetry. If the matrix elements are equal along the polarization direction of laser pulse, the even-order harmonics emerge. If they are opposite, the odd-order harmonics appear. For the z -component harmonics, the situation is the same as the x -component, as shown in Fig. 2(f).

C. Role of spin-orbit coupling

It is well known that the emergence of the 2D topological surface states in 6QL-Bi₂Se₃ is related to SOC [32]. Once SOC is taken into account in Cr-doped 6QL-Bi₂Se₃, spin up and spin down channels are mixed, the number of symmetry operations is reduced to 3: E , C_3^1 , and C_3^2 . Figures 3(a)-3(c) show HHGs from Cr-doped 6QL-Bi₂Se₃. The 3 symmetry operations are all the in-plane three-fold rotations C_3^n with the rotation axis along the z axis. When the laser fields are in-plane polarized, the even- and odd-order harmonics coexist for all the three components. This is because 3 symmetry operations belong to 3 subgroups. Each operation cannot cancel out any component harmonics. This is because each operation

changes the in-plane polarization of laser pulse. In other words, the laser pulse breaks the in-plane three-fold rotational symmetries C_3 . While the laser field is out-of-plane polarized, the in-plane component signals disappear, which is protected by the C_3 symmetry. We also notice that the symmetry properties of HHG have been investigated in monolayer MoS₂ and SiO₂, where the even harmonics are attributed to the broken inversion symmetry [3, 37].

D. Rules of HHG

Figure 4 summarizes our findings. There are three cases that are associated with the structural and magnetic differences: (i) native 6QL-Bi₂Se₃, (ii) Cr-doped 6QL-Bi₂Se₃ without SOC, and (iii) Cr-doped 6QL-Bi₂Se₃ with SOC. In (i), only odd harmonics, that are along the laser field \mathbf{E} , or the \parallel configuration, appear, while harmonics in the \perp configuration disappear. The latter requires the in-plane reflection symmetry. Here the laser field selects the symmetry operations to form a unit, which did hold the reflection symmetry. In (ii), in contrast to (i), there exist additional even-order harmonics for the components parallel to the x axis in both \parallel and \perp configurations, due to the broken inversion symmetry. (iii) represents an extreme case where both the inversion and reflection symmetries are broken. Each component contains both the even- and odd-order harmonics for any configuration. Our finding is generic and has important applications. For instance, based on the Haldane model [33], Chacon *et al.* recently reported that HHG contains both the even- and odd-order signals for the nontrivial topological phases [34], which are indeed realized through breaking the inversion symmetry. This is also the case for the Berry curvature to correct HHG [35], where the broken inversion symmetry plays a role. As demonstrated in Eq. (1), the inter-band transition dominates HHG. By contrast, the intra-band contribution, which is closely related to the topological phase as well as the Berry phase, only indirectly influences HHG. More advanced techniques are needed to test this prediction [36].

IV. CONCLUSION

We have demonstrated that high harmonic generation from six quintuple layers of Bi₂Se₃ carries rich information about its structure and group symmetry, regardless of whether it is doped or not. Harmonics from this topological insulator are complex in general. Although

traditional nonlinear optics has established the symmetry properties for low order harmonics, the entire procedure becomes increasingly difficult because there are too many possible combinations to be considered. We find a simple method by classifying all the symmetry operations into several subgroups that preserve the laser polarization. In our pristine undoped Bi_2Se_3 , the 12 symmetry operations form 3 subgroup, each of which consists of four symmetry operations. Depending on the laser polarization, these four symmetry operations are further grouped into two units. All the rules that we develop in Table I can be understood through this simple method. Physically, our method highlights the crucial interplay between the laser polarization and the material symmetry properties. We expect that this method will find broad applications in topological insulators and other technologically important materials.

ACKNOWLEDGMENTS

This work was supported by the National Science Foundation of China under Grant Nos. 11874189, 11774139 and 61674022. We also acknowledge the Fermi cluster at Lanzhou University for providing computational resources. GPZ was supported by the U.S. Department of Energy under Contract No. DE-FG02-06ER46304.

*sims@lzu.edu.cn

†guo-ping.zhang@outlook.com

-
- [1] T. Kanai, S. Minemoto, and H. Sakai, Quantum interference during high-order harmonic generation from aligned molecules, *Nature* **435**, 470 (2005).
 - [2] S. Ghimire and D. A. Reis, High-harmonic generation from solids, *Nat. Phys.* **15**, 10 (2019).
 - [3] H. Liu, Y. Li, Y. S. You, S. Ghimire, T. F. Heinz, and D. A. Reis, High-harmonic generation from an atomically thin semiconductor, *Nat. Phys.* **13**, 262 (2017).
 - [4] G. P. Zhang and Y. H. Bai, Magic high-order harmonics from a quasi-one-dimensional hexagonal solid, *Phys. Rev. B* **99**, 094313 (2019).
 - [5] N. Klemke, N. Tancogne-Dejean, G. M. Rossi, Y. Yang, F. Scheiba, R. E. Mainz, G. Di Sclaccia, A. Rubio, F. X. Kärtner, and O. D. Mücke, Polarization-state-resolved high-harmonic

- spectroscopy of solids, *Nat. Commun.* **10**, 1319 (2019).
- [6] J. Itatani, J. Levesque, D. Zeidler, H. Niikura, H. Pepin, J. C. Kieffer, P. B. Corkum, and D. M. Villeneuve, Tomographic imaging of molecular orbitals, *Nature* **432**, 867 (2004).
- [7] S. Ghimire, A. D. DiChiara, E. Sistrunk, P. Agostini, L. F. DiMauro, and D. A. Reis, Observation of high-order harmonics in a bulk crystal, *Nat. Phys.* **7**, 138 (2011).
- [8] G. Vampa and D. M. Villeneuve, High-harmonic generation: To the extreme, *Nat. Phys.* **11**, 529 (2015).
- [9] T. T. Luu, M. Garg, S. Yu. Kruchinin, A. Moulet, M. Th. Hassan, and E. Goulielmakis, Extreme ultraviolet high-harmonic spectroscopy of solids, *Nature* **521**, 498 (2016).
- [10] M. Garg, M. Zhan, T. T. Luu, H. Lakhota, T. Klostermann, A. Guggenmos, and E. Goulielmakis, Multi-petahertz electronic metrology, *Nature* **538**, 359 (2016).
- [11] S. Han, H. Kim, Y. W. Kim, Y.-J. Kim, S. Kim, I.-Y. Park, and S.-W. Kim, High-harmonic generation by field enhanced femtosecond pulses in metal-sapphire nanostructure, *Nat. Commun.* **7**, 13105 (2016).
- [12] C. L. Kane and E. J. Mele, Quantum spin Hall effect in graphene, *Phys. Rev. Lett.* **95**, 226801 (2005).
- [13] D. Hsieh, J. W. McIver, D. H. Torchinsky, D. R. Gardner, Y. S. Lee, and N. Gedik, Nonlinear optical probe of tunable surface electrons on a topological insulator, *Phys. Rev. Lett.* **106**, 057401 (2011).
- [14] H. K. Avetissian, A. K. Avetissian, B. R. Avchyan, and G. F. Mkrtchian, Multiphoton excitation and high-harmonics generation in topological insulator, *J. Phys. Condens. Matter.* **30**, 185302 (2018).
- [15] G. P. Zhang, M. S. Si, M. Murakami, Y. H. Bai, and T. F. George, Generating high-order optical and spin harmonics from ferromagnetic monolayers, *Nat. Commun.* **9**, 3031 (2018).
- [16] X.-L. Qi, T. L. Hughes, and S.-C. Zhang, Topological field theory of time-reversal invariant insulators, *Phys. Rev. B* **78**, 195424 (2008).
- [17] Y. L. Chen, J.-H. Chu, J. G. Analytis, Z. K. Liu, K. Igarashi, H.-H. Kuo, X.-L. Qi, S. K. Mo, R. G. Moore, D. H. Lu, M. Hashimoto, T. Sasagawa, S.-C. Zhang, I. R. Fisher, Z. Hussain, and Z. X. Shen, Massive dirac fermion on the surface of a magnetically doped topological insulator, *Science* **329**, 659 (2010).
- [18] C.-Z. Chang, J. Zhang, X. Feng, J. Shen, Z. Zhang, M. Guo, K. Li, Y. Ou, P. Wei, L.-L.

- Wang, Z.-Q. Ji, Y. Feng, S. Ji, X. Chen, J. Jia, X. Dai, Z. Fang, S.-C. Zhang, K He, Y. Wang, L. Lu, X. C. Ma, and Q. K. Xue, Experimental observation of the quantum anomalous Hall effect in a magnetic topological insulator, *Science* **340**, 167 (2013).
- [19] R. Yu, W. Zhang, H.-J. Zhang, S.-C. Zhang, X. Dai, and Z. Fang, Quantized anomalous Hall effect in magnetic topological insulators, *Science* **329**, 61 (2010).
- [20] P. Blaha, K. Schwarz, G. K. H. Madsen, D. Kvasnicka, and J. Luitz, *WIEN2k, An Augmented Plane Wave + Local Orbitals Program for Calculating Crystal Properties* (Karlheinz Schwarz, Techn. Universität Wien, Austria, 2001).
- [21] Y.-B. Hu, Y.-H. Zhao, and X.-F. Wang, Computational investigation of topological insulator Bi₂Se₃ film, *Front. Phys.* **6**, 760 (2014).
- [22] H. Zhang, C.-X. Liu, X.-L. Qi, X.-Y. Deng, X. Dai, Z. Fang, and S.-C. Zhang, Topological insulators in Bi₂Se₃, Bi₂Te₃ and Sb₂Te₃ with a single Dirac cone on the surface, *Nat. Phys.* **5**, 438 (2009).
- [23] See Supplemental Material at <http://link.asp.org/supplemental/>.
- [24] C. L. Tang and H. Rabin, Selection rules for circularly polarized waves in nonlinear optics, *Phys. Rev. B* **3**, 4025 (1971).
- [25] O. E. Alon, V. Averbukh, and N. Moiseyev, Selection rules for the high harmonic generation spectra, *Phys. Rev. Lett.* **80**, 3743 (1998).
- [26] X. Liu, X. Zhu, L. Li, Y. Li, Q. Zhang, P. Lan, and P. Lu, Selection rules of high-order-harmonic generation: Symmetries of molecules and laser fields, *Phys. Rev. A* **94**, 033410 (2016).
- [27] H. M. Nilsen, L. B. Madsen, and J. P. Hansen, On selection rules for atoms in laser fields and high harmonic generation, *J. Phys. B: At. Mol. Opt. Phys.* **35**, L403 (2002).
- [28] O. Neufeld, D. Podolsky, and O. Cohen, Floquet group theory and its application to selection rules in harmonic generation, *Nat. Comm.* **10**, 405 (2019).
- [29] N. Saito, F. Xia, F. Lu, T. Kanai, J. Itatani, and N. Ishii, Observation of selection rules for circularly polarized fields in high-harmonic generation from a crystalline solid, *Optica* **4**, 1333 (2017).
- [30] F. Langer, M. Hohenleutner, U. Huttner, S. W. Koch, M. Kira, and R. Huber, Symmetry-controlled temporal structure of high-harmonic carrier fields from a bulk crystal, *Nat. Photonics* **11**, 227 (2017).
- [31] T. Tamaya, A. Ishikawa, T. Ogawa and K. Tanaka, Diabatic mechanisms of higher-order

- harmonic generation in solid-state materials under high-intensity electric fields, *Phys. Rev. Lett.* **116**, 016601 (2016).
- [32] HHG from that including the surface states is featureless.
- [33] F. D. M. Haldane, Model for a quantum Hall effect without Landau levels: Condensed-matter realization of the “parity anomaly”, *Phys. Rev. Lett.* **61**, 2015 (1988).
- [34] A. Chacon *et al.*, Observing topological phase transitions with high harmonic generation, arxiv:1807.01616v2.
- [35] H. Liu, Y. Li, Y. S. You, S. Ghimire, T. F. Heinz, and D. A. Reis, High-harmonic generation from an atomically thin semiconductor, *Nat. Phys.* **13**, 262 (2017).
- [36] Dongbin Shin, Shunsuke A. Sato, Hannes, Hübener, Umberto De Giovannini, Jeongwoo Kim. Neojung Park, and Angel Rubio, Unraveling materials Berry curvature and Chern numbers from real-time evolution of Bloch states, *PNAS* **116**, 4135 (2019).
- [37] T. T. Luu and H. J. Wörner, Observing broken inversion symmetry in solids using two-color high-order harmonic spectroscopy, *Phys. Rev. A* **98**, 041802 (2018).

TABLE I: High harmonic generation is subject to both intrinsic symmetry operations and an extrinsic laser field. Under a linearly polarized laser pulse excitation, the 12 symmetry operations in 6QL-Bi₂Se₃ can be classified into 3 subgroups: SG_I, SG_{II}, and SG_{III}. Each subgroup contains four members of symmetry operations. When the symmetry of the crystal is lowered due to either magnetic doping or SOC, the number of symmetry operations is further reduced in each subgroup.

SG _I	SG _{II}	SG _{III}
$E = \begin{pmatrix} 1 & 0 & 0 \\ 0 & 1 & 0 \\ 0 & 0 & 1 \end{pmatrix}$	$C_3^1 = \begin{pmatrix} -1/2 & \sqrt{3}/2 & 0 \\ -\sqrt{3}/2 & -1/2 & 0 \\ 0 & 0 & 1 \end{pmatrix}$	$C_3^2 = \begin{pmatrix} -1/2 & -\sqrt{3}/2 & 0 \\ \sqrt{3}/2 & -1/2 & 0 \\ 0 & 0 & 1 \end{pmatrix}$
$\sigma_{xz} = \begin{pmatrix} 1 & 0 & 0 \\ 0 & -1 & 0 \\ 0 & 0 & 1 \end{pmatrix}$	$\sigma_1 = \begin{pmatrix} -1/2 & -\sqrt{3}/2 & 0 \\ -\sqrt{3}/2 & 1/2 & 0 \\ 0 & 0 & 1 \end{pmatrix}$	$\sigma_2 = \begin{pmatrix} -1/2 & \sqrt{3}/2 & 0 \\ \sqrt{3}/2 & 1/2 & 0 \\ 0 & 0 & 1 \end{pmatrix}$
$I = \begin{pmatrix} -1 & 0 & 0 \\ 0 & -1 & 0 \\ 0 & 0 & -1 \end{pmatrix}$	$IC_3^1 = \begin{pmatrix} 1/2 & -\sqrt{3}/2 & 0 \\ \sqrt{3}/2 & 1/2 & 0 \\ 0 & 0 & -1 \end{pmatrix}$	$IC_3^2 = \begin{pmatrix} 1/2 & \sqrt{3}/2 & 0 \\ -\sqrt{3}/2 & 1/2 & 0 \\ 0 & 0 & -1 \end{pmatrix}$
$R_y = \begin{pmatrix} -1 & 0 & 0 \\ 0 & 1 & 0 \\ 0 & 0 & -1 \end{pmatrix}$	$I\sigma_1 = \begin{pmatrix} 1/2 & \sqrt{3}/2 & 0 \\ \sqrt{3}/2 & -1/2 & 0 \\ 0 & 0 & -1 \end{pmatrix}$	$I\sigma_2 = \begin{pmatrix} 1/2 & -\sqrt{3}/2 & 0 \\ -\sqrt{3}/2 & -1/2 & 0 \\ 0 & 0 & -1 \end{pmatrix}$

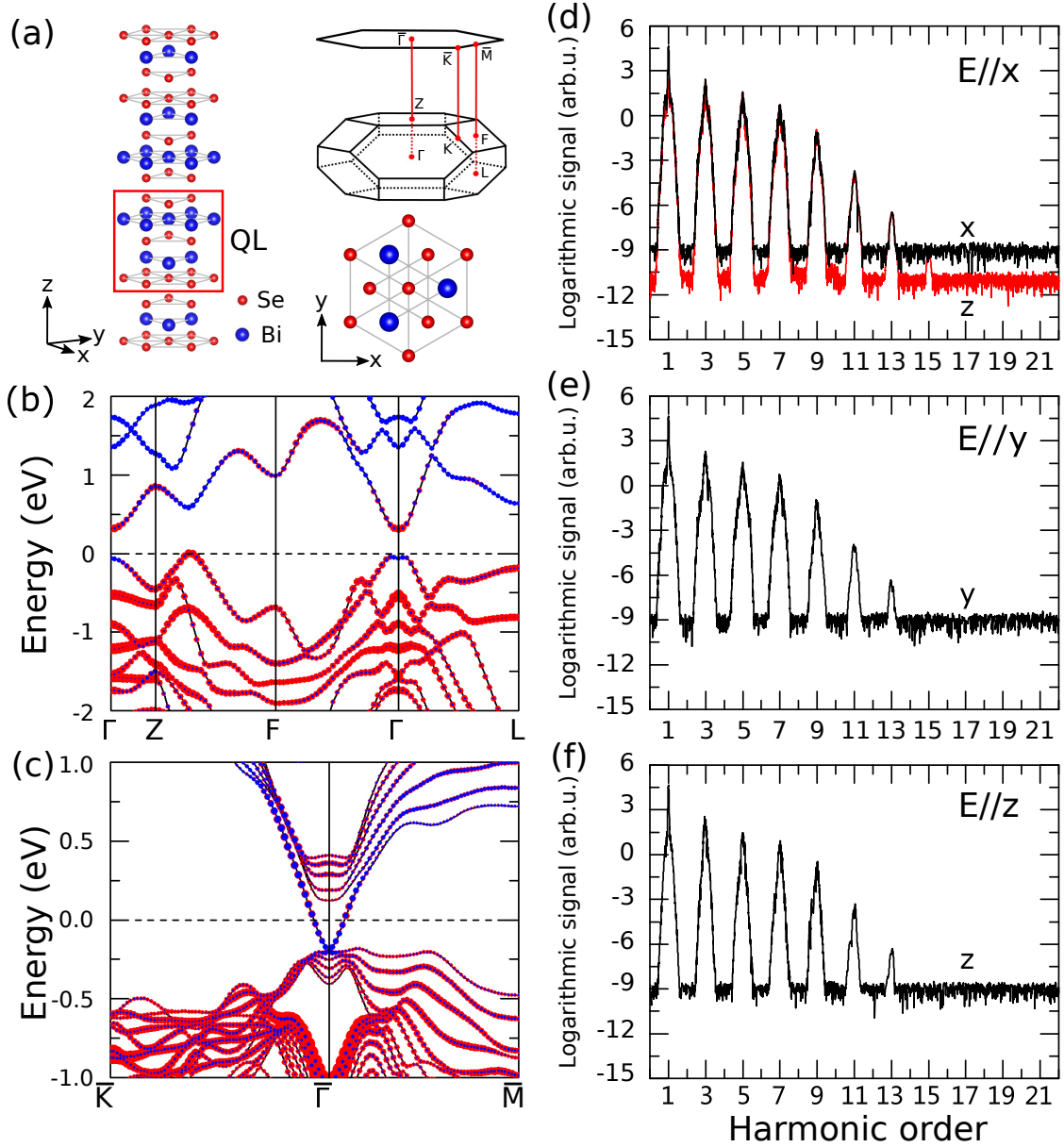


FIG. 1: (a) Structure of Bi_2Se_3 . The red rectangle is the repeated quintuple cells. Red and blue spheres represent Se and Bi atoms, respectively. Top right panel: bulk Brillouin zone (BZ) and (111) surface BZ of the Bi_2Se_3 , with high symmetry points (Γ , Z, F, L, $\bar{\Gamma}$, \bar{M} , and \bar{K}) identified. Bottom right panel: the projection on the ab plane of Bi_2Se_3 . (b) Element-resolved band structure of bulk Bi_2Se_3 , where red and blue circles represent the Se and Bi atoms, respectively. (c) Surface electronic structure of 6QL- Bi_2Se_3 . The red and blue circles represent the Se and Bi atoms in the top and bottom QLs, respectively. (d)-(f) High harmonic signals for 6QL- Bi_2Se_3 with laser polarization along the (d) x , (e) y and (f) z axes. The photon energy of the laser field is $\hbar\omega = 1.5$ eV, with duration $\tau = 60$ fs and vector potential amplitude $A_0 = 0.03$ Vfs/Å. Signals at noise level are not shown.

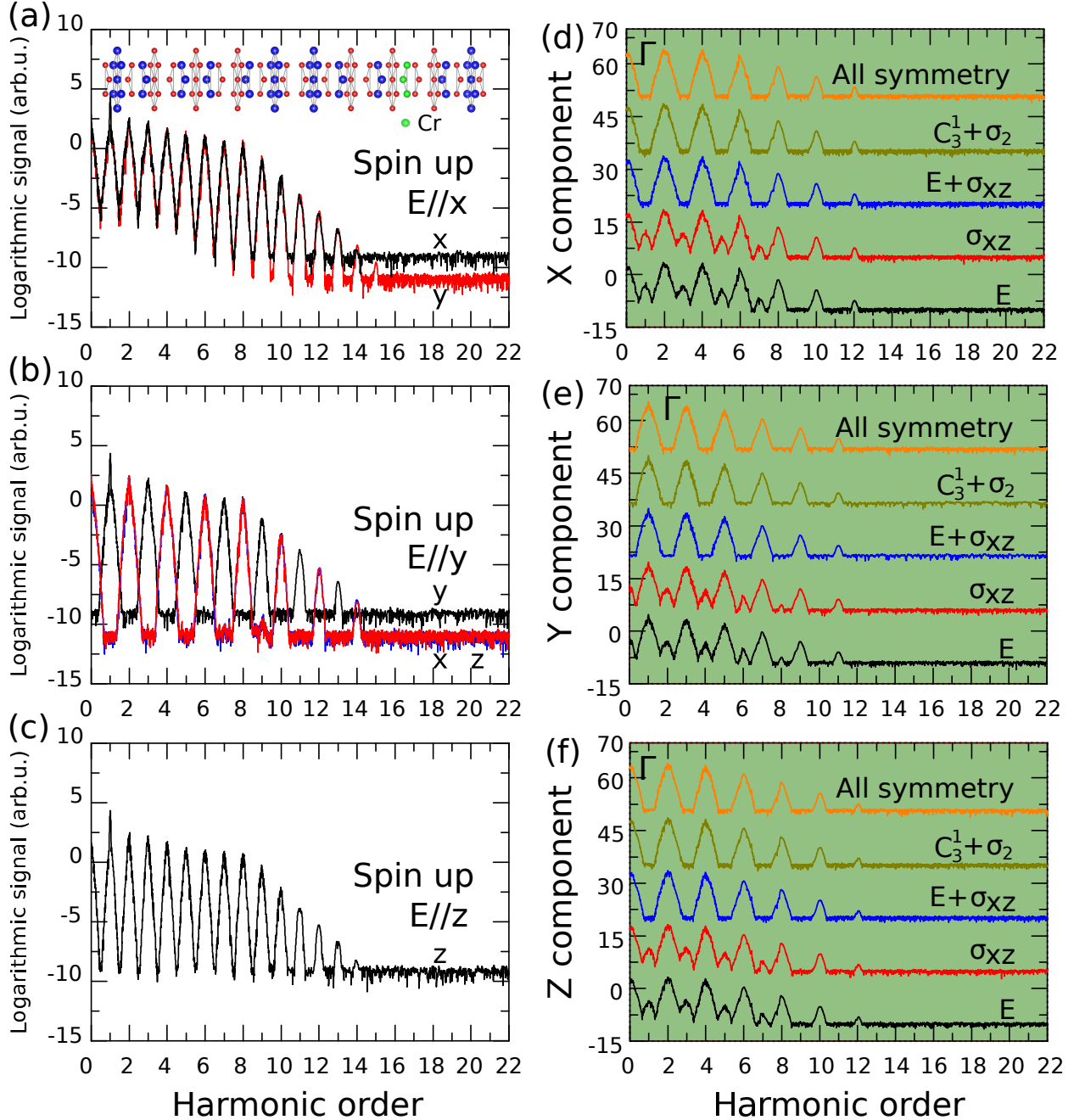


FIG. 2: Harmonic signals from the spin up channel of Cr-doped 6QL-Bi₂Se₃ for the laser polarization along the (a) x axis, (b) y , and (c) z axes. The inset in (a) is the structure of Cr-doped 6QL-Bi₂Se₃. The photon energy is taken as $\hbar\omega = 1.0$ eV to excite the electronic states near the Fermi level. Other parameters of the laser are the same as those in Fig. 1. (d), (e) and (f) use the laser polarization along the y axis. (d) Symmetry-resolved harmonic signal along the x axis from the Γ point alone. Symmetry operations that enter the calculation are given above each of the curves. For clarity, all the spectra, except the bottom one, are shifted vertically. (e) Same as (d), but with the harmonic signal along the y axis. (f) Same as (d), but with the harmonic signal along the z axis.

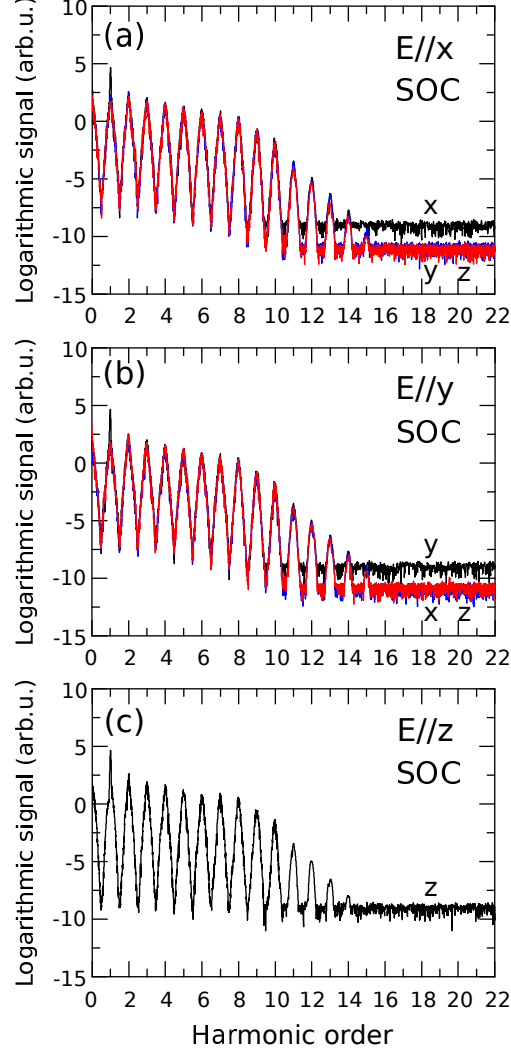


FIG. 3: Harmonic spectra from Cr-doped 6QL-Bi₂Se₃ in the presence of spin-orbit coupling. (a) The laser polarization is along the x axis. In the presence of spin-orbit coupling, the group symmetry is reduced, the inversion symmetry is broken and even harmonics appear. The harmonic signals are also generated along the z axis, which is very different from that in Fig. 2(a). The laser parameters are the same as in Fig. 2. (b) Laser-polarization is along the y axis. The results are similar to Fig. 2(b). (c) Laser-polarization is along the z axis.

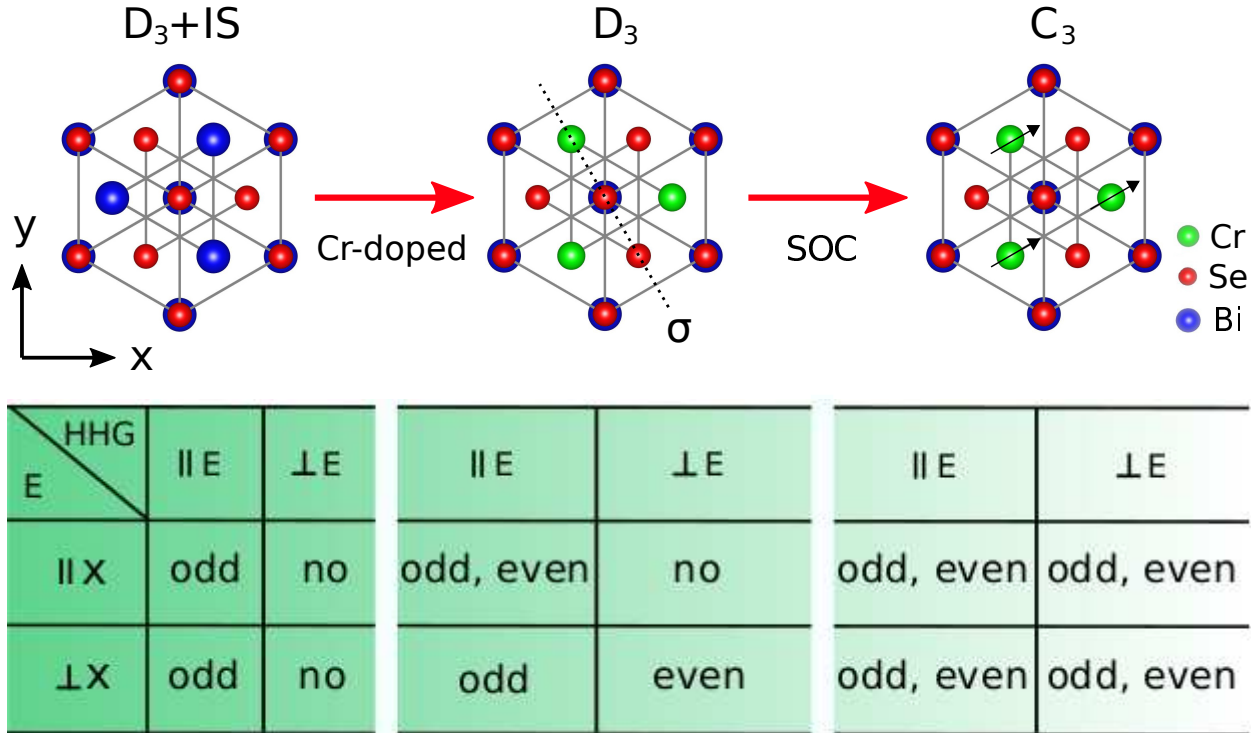


FIG. 4: Symmetry properties of HHG signals under two configurations \parallel and \perp . From left to right are for the pristine structure, Cr-doped structure, and Cr-doped structure with spin-orbit coupling. The bottom panel shows the rules how harmonic signals are emitted. IS denotes the inversion symmetry, which is broken by magnetic doping. SOC breaks the in-plane reflection symmetry (σ), where the spin of Cr atoms (the arrows) plays a role.